

Onboard Image Processing by Inverse Filtering

V.E. Kvitka, *postgraduate student, kva-vasja@yandex.ru*

Joint Stock Company "Space Rocket Centre "Progress" –

*Scientific and Production Enterprise "OPTEKS", Zelenograd, Moscow, Russian Federation
Moscow Institute of Physics and Technology, Dolgoprudny, Moscow Region, Russian Federation*

V.D. Blinov, *v_blinov@mail.ru*

Joint Stock Company "Space Rocket Centre "Progress" –

Scientific and Production Enterprise "OPTEKS", Zelenograd, Moscow, Russian Federation

Abstract. Satellite images of the Earth of high resolution have blurring of small details and low contrast. This is due to the low values of the modulation transfer function of the large space-based optical Earth observation systems. The problems of image reconstruction by the inverse filtering method are considered in the article. Various ways of its implementation are suggested. The necessity of preliminary noise reduction of images before their restoration is revealed. A quantitative and qualitative analysis of the performance of the most well-known noise reduction algorithms has been performed. Adaptive algorithms of preliminary noise reduction are developed and tested. By computer simulation of images and comparison of quality criteria, the optimal algorithm of preliminary noise reduction of images is for this task is discovered. Regularization, an alternative solution to the problem of noise amplification in an image when performing inverse filtering is studied. A computer simulation of various regularization methods has been carried out. Visual analysis of the results of image modeling and comparison of quantitative criteria for their quality made it possible to determine the optimal parameters of the regularization function.

Keywords: noise reduction, inverse filtering, modulation transfer function

Problem definition

One of the properties of high-resolution Earth remote sensing spacecraft (ERS SC) is the low value of the modulation transfer function (MTF) at high spatial frequencies. Visually this is manifested in the blurring of images of small objects [1]. Let us investigate the possibility of improving the image by inverse filtering performed onboard a spacecraft.

As is well known, the modulation transfer function $MTF(\nu)$ relates the Fourier image of $F(\mathbf{A})$ of the original image \mathbf{A} and the Fourier image $F(\mathbf{B})$ of the image \mathbf{B} obtained by an optoelectronic system, which is shown by equation (1). Here and in what follows, we are talking about a two-dimensional discrete Fourier transformation (2DDFT).

$$F(\mathbf{B}) = F(\mathbf{A}) \cdot MTF(\nu). \tag{1}$$

Naturally, a suggestion arises to restore image \mathbf{A} , having image \mathbf{B} obtained by a HR SC surveying the Earth's surface. We carry this out by the formula (2):

$$\mathbf{A} = F^{-1} \left(\frac{F(\mathbf{B})}{MTF(\nu)} \right). \tag{2}$$

However, the implementation of this method, known as inverse filtering, has a great practical difficulty: for small values of $MTF(\nu)$, the noise always present in image \mathbf{B} will lead to strong distortions of the reconstructed image \mathbf{A} [2]. Accordingly, the question arises of investigating the limits of applicability of this method of image reconstruction. The key point is the need to perform the procedure not on the Earth, but on board a spacecraft.

Otherwise, there will be additional distortions associated with the operation of the video compression algorithm.

Image simulation

The procedure of the image simulation is based on the use of aerial photographs with a 12-bit brightness gradation. Since inverse filtering is considered for a high-resolution spacecraft (about 0.5 m), it is necessary that the original images have a significantly smaller pixel projection. Otherwise, a visual analysis of the results of inverse filtering will be incorrect, since the MTF of the air camera, which is significantly different from 1, will introduce its distortions. Therefore, aerial photographs with L_{aer} pixel projection of not more than 0.2 m are used for the modeling.

Let's note its main stages:

1. The pixel projection of the aerial photograph L_{aer} is calculated, after which it is rescaled to the projection of the pixel L_{sc} (scaling factor $k = L_{aer} / L_{KA}$). The results of this operation are described by the matrix \mathbf{A} .

2. The modulation transfer function (MTF) of the optoelectronic path $MTF(\nu)$ is shown in Fig. 1.

3. 2DDFT of the snapshot \mathbf{A} is performed. We denote the result as $F(\mathbf{A})$.

4. We simulate the blurring of small details of the image \mathbf{A} by multiplying the spectrum $F(\mathbf{A})$ by the MTF of the optoelectronic tract $MTF(\nu)$. The result $F(\mathbf{B}) = F(\mathbf{A}) \cdot MTF(\nu)$ is the Fourier spectrum of the image \mathbf{B} formed in the focal plane of the telescope. Accordingly, in order to obtain the image \mathbf{B} , it is necessary to perform the reverse 2DDFT using formula (3):

$$\mathbf{B} = F^{-1}(F(\mathbf{B})) = F^{-1}(F(\mathbf{A}) \cdot MTF(\nu)). \tag{3}$$

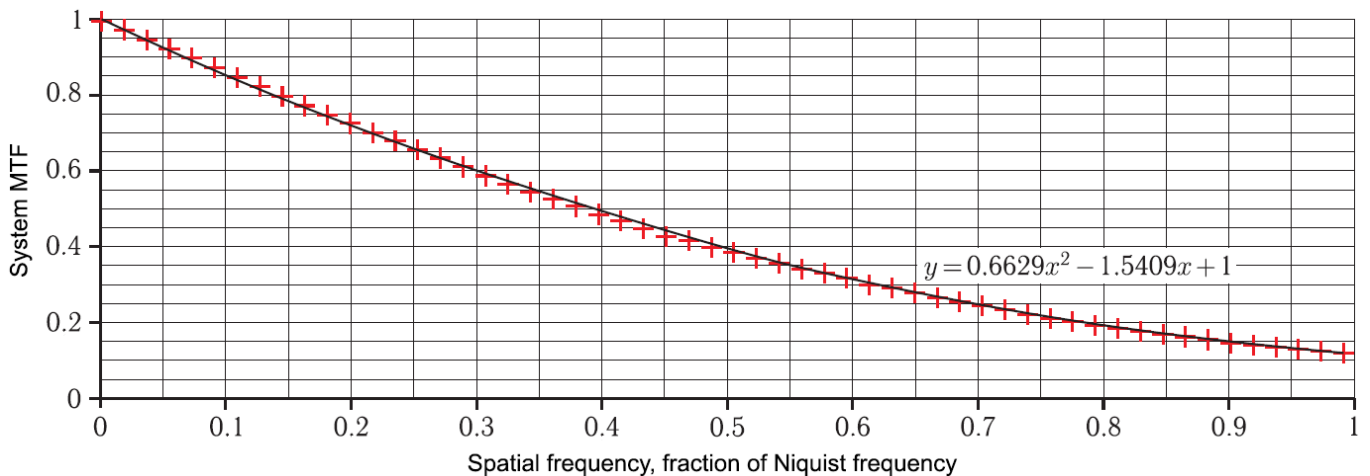


Fig. 1. Modulation transfer function of the system and its approximation.



Fig. 2 (Image A)



Fig. 3 (Image B)



Fig. 4 (noisy image C)

5. We simulate the noise of image B taking into account the photon noise, based on the energy calculation of the spacecraft for the corresponding height of the Sun above the horizon. Then the RMS of the noise has its own value for each pixel. We denote the result as C.

Here we apply a dimensionless spatial frequency normalized to the Nyquist frequency (55.56 pairs of lines per mm).

Figures 2-4 show fragments of the resampled aerial photograph A, the image on the focal plane of the objective B and the noisy image C, respectively, at the sun height $h_s=5^\circ$. All three images include four groups of three test objects on the upper left (high and low contrasts, periods of 2 and 4 pixels).

Study of inverse filtering

We perform inverse filtering without prior noise reduction for images C (h_s), noisiness of which corresponds to different elevations of the Sun over the horizon h_i . The restored image of A_{inv} is described by the formula (4):

$$A_{inv} = F^{-1} \left(\frac{F(C)}{MTF(\nu)} \right). \quad (4)$$

The result is shown in Figure 5, where enlarged fragments of the images are shown

It can be seen from Fig. 5 that a satisfactory result of inverse filtering can be obtained only at elevations of the Sun exceeding $h_s = 30^\circ$, when the noisiness of the images is low. We shall produce image C_{fl} using noise reduction and apply inverse filtering to it. The results are shown in Figure 6.

It can be seen from Fig. 6 that the best result is provided by inverse filtering of an image with noise reduction performed using the pseudo-median filter described in [3]. In this method, the pixel signal is replaced by $\text{med}(y_1, y_2, y_3)$, where y_1, y_2, y_3 are the median signal values in the rows of the 3×3 pixel window. Restoration after the median noise filtering has caused distortion of the image of the test object, and the geometric average filter blurs the details to such a degree that the inverse filtering is unable to restore the sharpness of the edges.



a) Original image C,
 $h_s=5^\circ$



b) Restored image A_{inv} ,
 $h_s=2^\circ$



c) Restored image A_{inv} ,
 $h_s=30^\circ$

Fig. 5 Inverse filtering without prior noise reduction

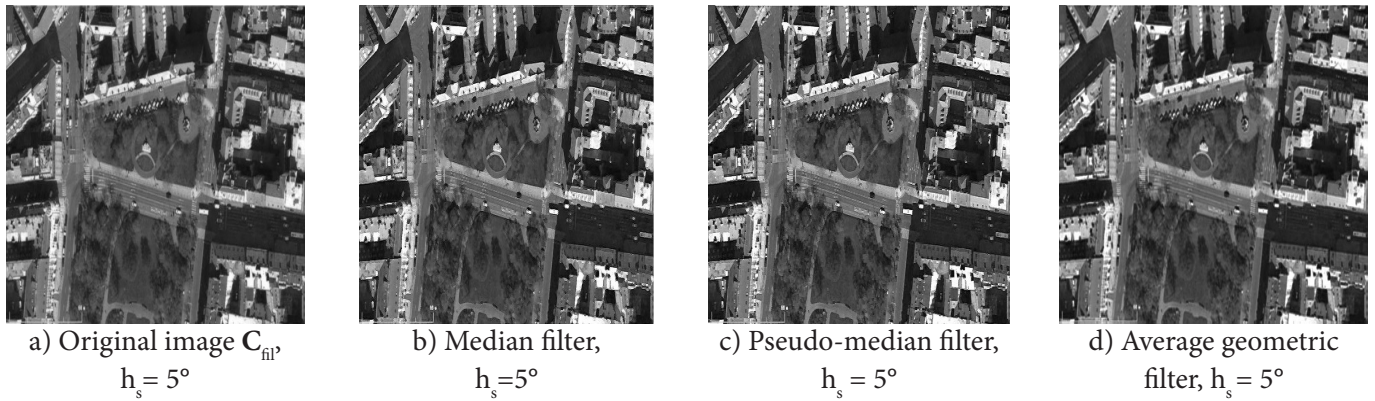


Fig. 6. Results of noise reduction and subsequent inverse filtering

Preliminary processing with adaptive filter

We investigate the inverse filtering performed on the image, which has undergone noise reduction by the adaptive algorithm. The idea of such a filter is described in [2, p. 355]. It should take into account the dependence of RMS of the noise on the signal in a pixel, and in the presence of strong luminance differences it should not smooth them, since these are not noise, but the outlines of the objects.

The following algorithm is proposed: as a sign of the presence of contours in the 3x3 pixel window **E**, we shall assume as a requirement that $RMS^2(\mathbf{E}) / noise^2(i,j) \geq 9$. That is, the actual RMS of the noise in the 3x3 pixel window is 3 times larger than the noise in pixel **C**(i, j). A flowchart of the algorithm is shown in Figure 7.

In this case, the noise RMS is calculated by the on-board device according to the formula (5):

$$noise(i, j) = \frac{4095}{P_{zap}} \cdot \sqrt{C(i, j) \cdot \frac{P_{ch}}{4095}} \tag{5}$$

The charge capacity of the photodetector P_{ch} is known in advance. However, the calculation of the squared value of the RMS of the signal in the 3x3 pixel window requires about 20 operations, which is too many for an on-board processing task.

Detecting outlines using a gradient

We shall use for noise reduction a gradient algorithm that takes into account the direction of the contours in the sliding window of 3x3 pixels. As is known, the gradient of a function of two variables $U(x, y)$ is the vector that determines the direction of the greatest change in the function. If there is a contour in the window, the vector gradient will be perpendicular to the sharp edge. Then

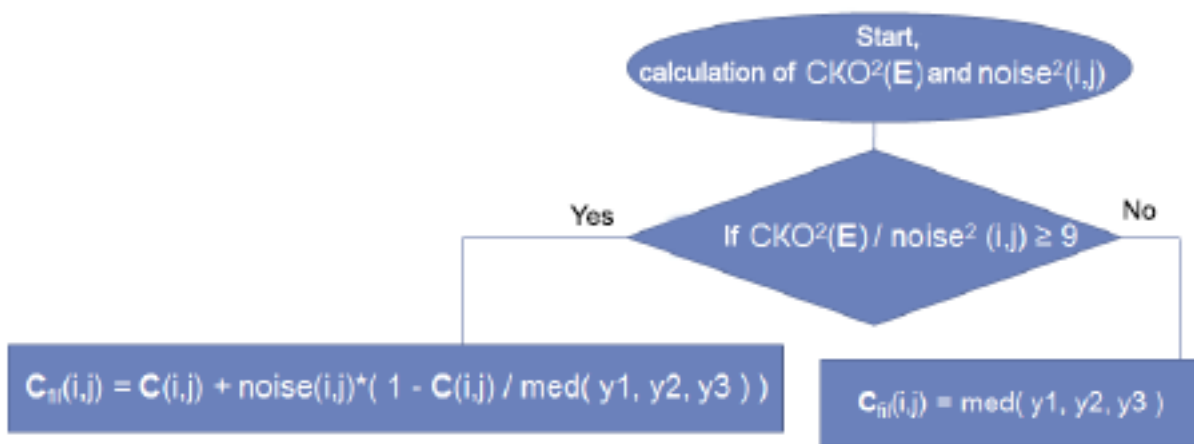


Fig. 7. Flowchart of the algorithm.

we average the brightness of the pixels exactly in the direction of the contour to prevent it from blurring. Mathematically, this is described by formula (6).

$$C_{\text{fil}}(i, j) = a \cdot C(i, j) + b \cdot \left(\sin^2 \theta \cdot \frac{C(i, j - 1) + C(i, j + 1)}{2} + \cos^2 \theta \cdot \frac{C(i - 1, j) + C(i + 1, j)}{2} \right). \quad (6)$$

In this case, the condition $a + b = 1$, which is necessary for the invariance of the average brightness of the image of a homogeneous surface, is satisfied. The angle θ , which is the angle between the gradient vector and the X axis, is determined by the formula (7):

$$\text{tg } \theta = \frac{\frac{\partial U}{\partial y}}{\frac{\partial U}{\partial x}} = \frac{C(i + 1, j) - C(i, j)}{C(i, j + 1) - C(i, j)}. \quad (7)$$

Then $\sin^2 \theta = \frac{\text{tg}^2 \theta}{1 + \text{tg}^2 \theta}$, and $\cos^2 \theta = \frac{1}{1 + \text{tg}^2 \theta}$.

These equations make it possible to avoid the time-consuming calculation of the sine and cosine by the Taylor series expansion method.

Note that the corner pixels of the 3x3 window are not involved in the calculations. To improve the transmission of non-horizontal and non-vertical contours, we introduce into the algorithm a branch that takes into account the angular pixel values of the 3x3 pixel window. A flowchart of the gradient noise reduction algorithm is shown in Figure 8.

When considering the diagonal contour $30^\circ < |\theta| < 60^\circ$, one of the branches works when the contour can be considered diagonal and at the upper part of the 3x3 window the contour is at the top, and in the right part of the window the contour is at the bottom. Similarly, the other branch works if the diagonal contour is at the bottom of the 3x3 window. The results of applying the algorithm with the values of the parameters $a = 0.5$ and $b = 0.5$ are shown in Figures 9-11.

As can be seen from Figures 9-11, at a height of the sun exceeding 10 degrees, a completely acceptable result of inverse filtering is provided.

Laplacian based noise reduction

The contours and inhomogeneities in the 3x3 window can be detected using the Laplacian operator. It is defined by the equation (8):

$$\begin{aligned} \text{Lap}(i, j) &= \left| \frac{\partial^2 U}{\partial x^2} + \frac{\partial^2 U}{\partial y^2} \right| = \\ &= \left| (C(i, j - 1) + C(i, j + 1) - 2 \cdot C(i, j)) + \right. \\ &\quad \left. + (C(i - 1, j) + C(i + 1, j) - 2 \cdot C(i, j)) \right|. \end{aligned} \quad (8)$$

Obviously, for a white dot on a black background, it results in $\text{Lap}(i, j) = 2 \cdot |0 + 0 - 4095| = 8190$. For an absolutely sharp horizontal white line on a black background, we have $\text{Lap}(i, j) = |0 + 0 - 4095| = 4095$.

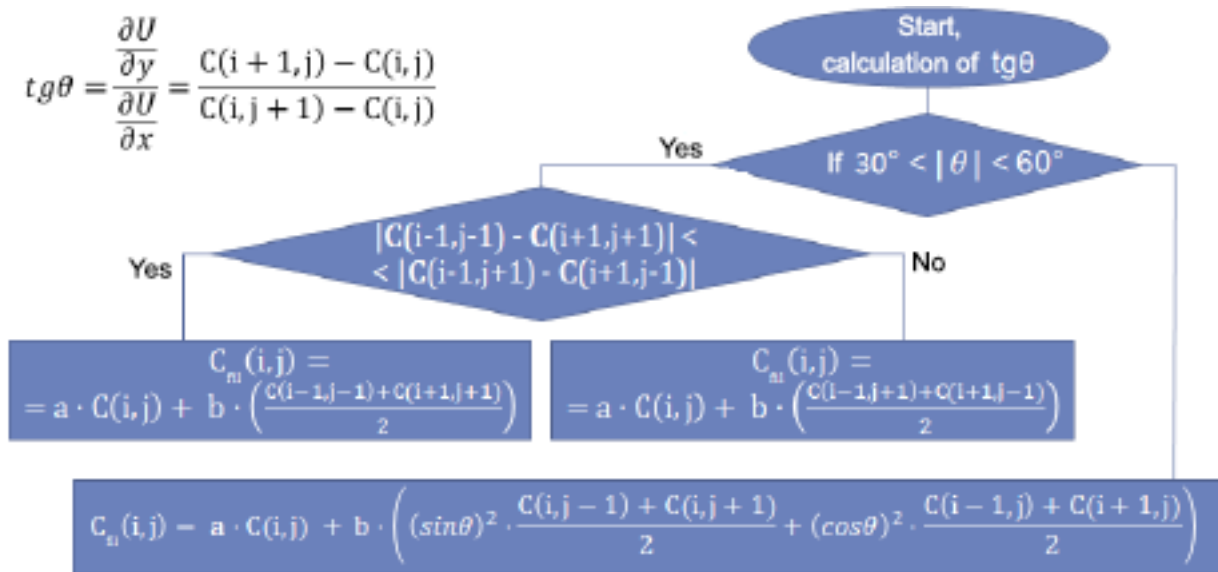


Fig. 8. Flowchart of the gradient noise reduction algorithm.



Fig. 9. $a=0,5; h_s=2^\circ$



Fig. 10. $a=0,5; h_s=5^\circ$



Fig. 11. $a=0,5; h_s=10^\circ$

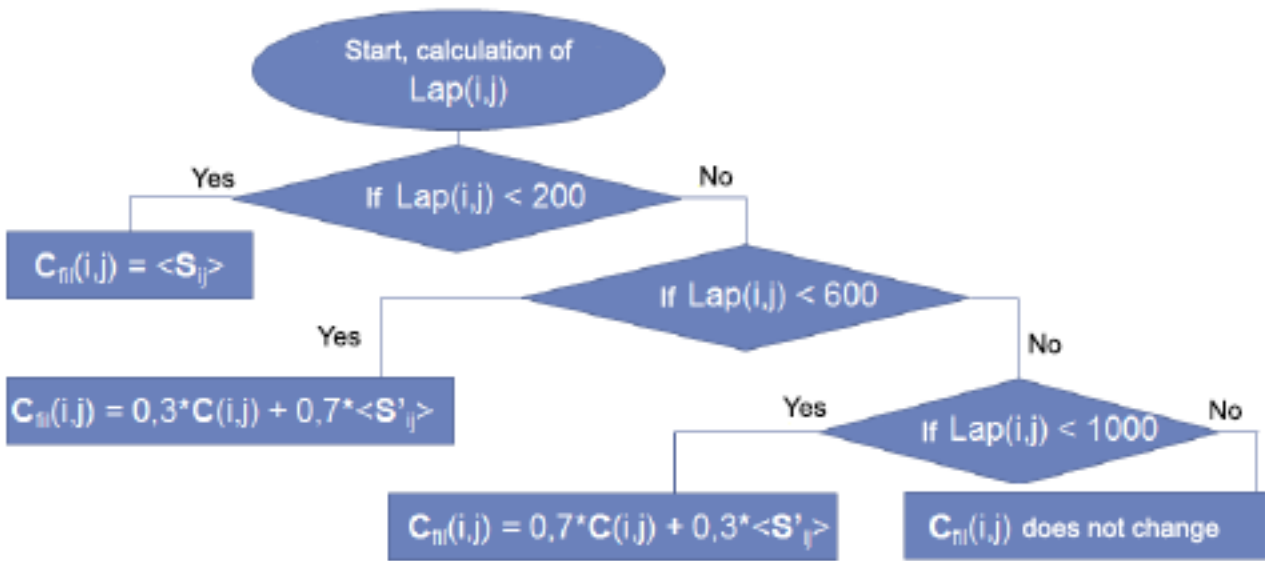


Fig. 12. Flowchart of the Laplacian noise reduction algorithm.

Consider an algorithm based on the three threshold values of the Laplacian at the current point of the image $C(i, j)$. The flowchart is shown in Fig. 12.

Here S_{ij} is a 3x3 pixel window, and S'_{ij} is the surroundings of the point (i, j) , that is, the 3x3 window without the central pixel. Accordingly, $\langle S_{ij} \rangle$ is the average value of the signal of 9 pixels, and $\langle S'_{ij} \rangle$ is the average value of 8 pixels.

Thus, we prevent the changing of the signal at points with very strong local inhomogeneities $(Lap(i, j) \geq 1000)$ to avoid blurring of small details. On the contrary, for equiluminous sections, a branch of the algorithm that averages all 9 pixels of the window with the same weights is used.

We apply the described algorithm for the preliminary noise reduction performed before inverse filtering. The result of obtaining of the A_{inv} images for different elevations of the Sun is shown in Fig. 13–14.

As can be seen from Fig. 13-14, the result of image restoration using this algorithm of preliminary noise cancellation is worse than using the gradient method, since there are individual dark or light points in homogeneous areas.

Resolution regularization

In addition to the use of adaptive noise reduction algorithms, the problem of dividing the Fourier image by a small value of the MTF can be solved by regularizing the solution described in [4]. The idea of regularization is described by formula (9):

$$A_{inv} = F^{-1} \left(\frac{F(C)}{MTF(\nu) + Reg(\nu)} \right), \quad (9)$$

Where: $Reg(\nu)$ is the regularization function.

From the analysis of formula (9) we can formulate two requirements for the regularization function:



Fig. 13. $A_{inv}, h_s=2^\circ$



Fig. 14. $A_{inv}, h_s=10^\circ$



a) $\alpha = 0.01$



b) $\alpha = 0.5$



c) $\alpha = 2$

Fig. 15. Simulation of inverse filtering without prior noise cancellation

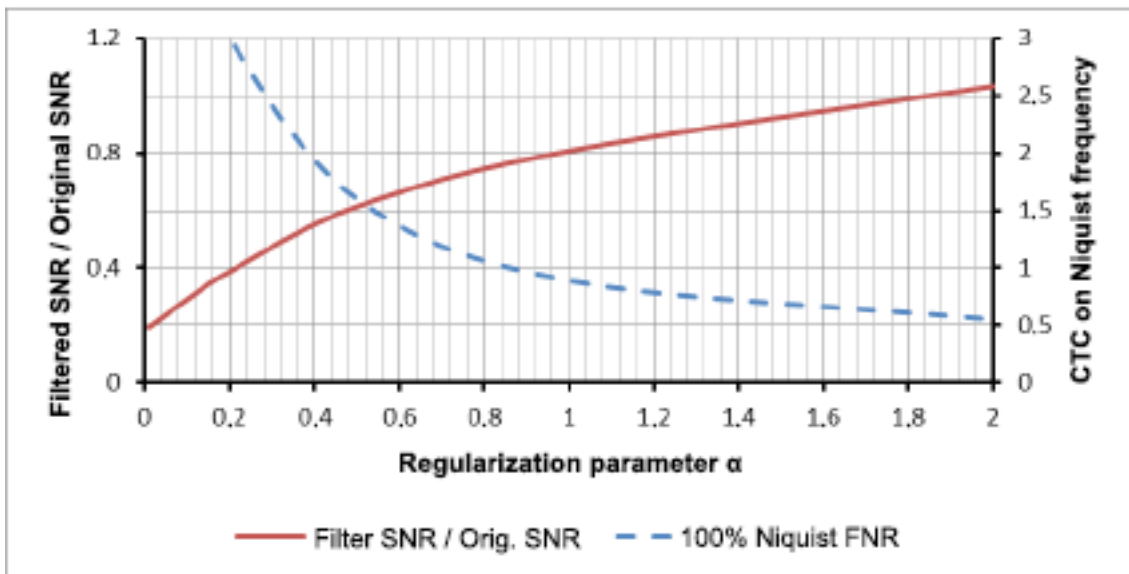


Fig. 16. Dependences of the contrast transfer coefficient (CTC) and the change in signal-to-noise ratio (SNR after filtering / SNR initial) on the coefficient α .

$Reg(0) = 0$, since at small spatial frequencies the distortions are minimal and regularization is not needed.

$Reg(1)$ must be non-zero, but not close to 1, so as not to allow large distortion of the restored image.

The use of regularization instead of the preliminary noise cancellation is of interest, since it requires fewer operations with the data array. We analyze various variants of the regularization function.

Quadratic dependence

$Reg(v) = \alpha \cdot vt^2$, where α is the experimentally chosen dimensionless coefficient. We will try to experimentally optimize the value of α . Figure 15 shows the simulation of inverse filtering for different α values without prior noise cancellation.

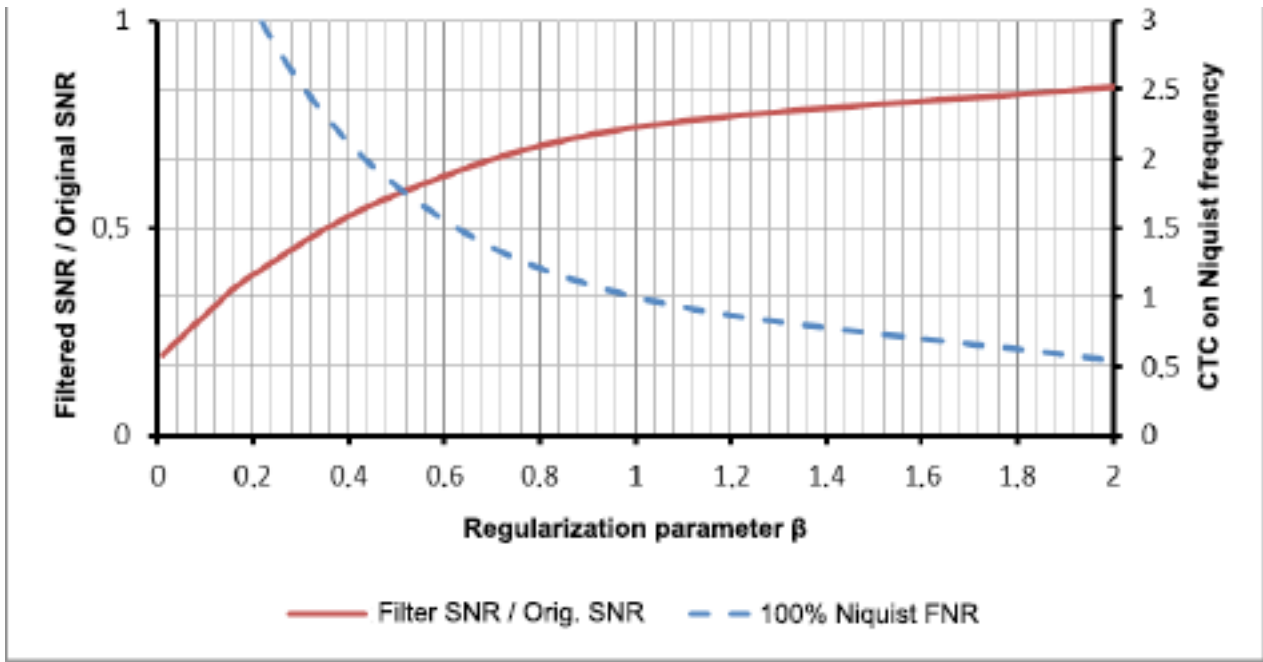


Fig. 17. Dependencies of the CTC and changes in the signal-to-noise ratio (SNR after filtration / SNR initial) from the coefficient β .

Table 1. Main characteristics of inverse filtering options

pre-noise reduction variant	SNR ₅₀		FNR	
	in the source image	on the processed image	0.5 v _N	v _N
without noise reduction	31	5.6	3	8.6
pseudo-median	31	15	2.4	-5
gradient algorithm	31	9	3	7
Laplacian algorithm	31	21	3.7	8.6
regularization $\alpha \cdot v^2$ ($\alpha = 0.8$)	31	$31 \cdot 0.7=22$	1	1
the regularization $\beta \cdot v^3$ ($\beta=1$)	31	$31 \cdot 0.75=23$	1	1

When analyzing Figures 15a-15c, it is seen that as the α increases, the signal-to-noise ratio increases, but the contrast decreases. The nature of this relationship is shown in Fig. 16. Next, we will talk about the signal-to-noise ratio given for a signal that is half of the maximum, which corresponds to an albedo of 0.5. Denote this value SNR₅₀.

Assuming that the CTC should be close to 1, like the change in SNR, we determine that the optimal value of α is in the range from 0.6 to 1.

Cubic Dependence

Consider another regularizing function: $Reg(v) = \beta \cdot v^3$, where β is the experimentally selectable dimensionless coefficient. Then the effect of the change in the denominator of fraction (3) at low frequencies will be less than for quadratic regularization. Figures 23a - 23c show the simulation of inverse filtering without noise reduction. Analogously to the quadratic regularization, the signal-to-noise ratio increases with increasing β , but

the CTC falls off. The nature of this relationship is shown in Figure 17.

Assuming that the contrast transfer coefficient should be close to 1, like the change in SNR, we find that the optimal value of β is in the range from 0.8 to 1.2.

Conclusion

For a mathematical description of the quality of inverse filtering, let us summarize in Table 1 the main characteristics of its variants. Here FNR ($0.5 \nu_N$) is the ratio of the target object image contrasts with a spatial frequency of 50% of the Nyquist frequency for the processed and original images. The negative value of the FNR corresponds to the inversion of the bars of the test object: the black bar becomes white and vice versa. A similar phenomenon can be observed in Figure 6 with pseudo-median filtration.

Let us analyze the data in Table 1 and the results of preliminary noise reduction algorithms. Optimal solutions for image preparation are the use of the gradient method of noise reduction or cubic regularization. In addition, it is possible to use these operations jointly when the regularization is performed on the Fourier image that underwent noise reduction.

References

1. Baklanov A.I. *Sistemy nablyudeniya i monitoringa: uchebnoe posobie* [Monitoring and monitoring systems: textbook]. Moscow, BINOM. Laboratoriya znaniy, 2009, 234 pp. (in Russian)
2. Gonsales R., Vuds R. *Tsifrovaya obrabotka izobrazheniy* [Digital image processing]. Moscow, Tekhnosfera, 2005, 1072 pp. (in Russian)
3. Akinshin N.S., Esikov O.V. Pseudomediannaya fil'tratsiya dlya obrabotki opticheskikh izobrazheniy [Pseudo-median filtering for processing optical images]. *Materialy XII nauchno-tekhnicheskoy konferentsii "Sistemy nablyudeniya, monitoringa i distantsionnogo zondirovaniya Zemli"* [Proceedings of the XII Scientific and Technical Conference "Systems of Earth observation, monitoring and remote sensing"]. Kaluga, Manuskript, 2015, 436 pp. (in Russian)
4. Kashkin V.B., Sukhinin A.I. *Tsifrovaya obrabotka aerokosmicheskikh izobrazheniy* [Digital processing of aerospace images]. Digital resource, a summary of lectures. Krasnoyarsk, IPK SFU, 2008. (in Russian)